*Solid State Science and Technology, Vol. 33, No. 2 (2025) 149-160*
*https://doi.org/10.66514/ssst33-2-149-160*

# Modulating Pseudo Confinement in Type-II Core-Shell Quantum Dots

Nur Ain Arina Abd Hamid[1], Nurisya Mohd Shah[1,2] *, Chan Kar Tim[1,2], Amsyar Rahim[1]

[1]*Department of Physics, Faculty of Science, Universiti Putra Malaysia, 43400 UPM Serdang, Selangor, Malaysia*
[2]*Institute for Mathematical Research (INSPEM), Universiti Putra Malaysia, 43400 UPM Serdang, Selangor, Malaysia*

**Corresponding author (email: risya@upm.edu.my)*

*(Received: 25 August 2025 / Revised: 3 December 2025 / Accepted: 5 January 2026 / Published online: 8 January 2026)*

## ABSTRACT

We investigated the transition energy modulation in type-II core-shell quantum dots (CSQDs) using a single-band step-potential framework. By analyzing radial probability densities and quantum transmission coefficients, we classify carrier confinement regimes as strong or weak based on potential barriers and localization behavior. Applied to PbS/CdS and ZnTe/ZnSe heterostructures, our model reveals that strong confinement enhances transition energies via suppressed tunneling and sharp wavefunction localization. In contrast, weak confinement allows partial delocalization, leading to a step-defined pseudo-type-II regime where hole behavior exhibit type-I-like hole localization despite type-II band alignment. These findings provide theoretical insight into tuning near-infrared transition energies and carrier lifetimes for quantum dot optoelectronic applications.

Keywords: Quantum confinement; radial probability; transmission coefficient; type-II core-shell quantum dot

## INTRODUCTION

Core-shell quantum dots (CSQDs) offer a powerful platform for tuning the optical and electronic properties of semiconductor nanostructures through material selection and spatial confinement. Challenges remain in their synthesis and integration into commercial devices for application in photovoltaic technology as QD sensitized solar cells [1] and optoelectronics [2, 3]. Traditionally, CSQDs are categorized into type-I or type-II systems based on their band alignment: in type-I, both carriers are confined within the core [4], while in type-II, the electron and hole are spatially separated across the core-shell interface [5]. While this classification captures general carrier localization trends, it often overlooks the elegant interplay between potential barrier depth, effective mass mismatch, and quantum confinement strength especially in systems with finite step-like potential

profiles. Such subtleties can give rise to regimes where the carrier distribution deviates from the expected type-II behavior, despite the underlying band offsets [3,6]. This motivates the need to refine the conventional classification by examining confinement behavior beyond simple energetic alignment.

In this work, we present a theoretical framework to characterize confinement behavior in type-II CSQDs by combining radial probability analysis, quantum transmission coefficients, and numerically obtained transition energies. We model the carriers using a single-band step-potential approach that captures finite barrier effects at the core-shell interface, enabling us to resolve both strong and weak confinement regimes. As case studies, we analyze two experimentally relevant heterostructures: PbS/CdS, which exhibits pronounced band offsets leading to strong confinement, and ZnTe/ZnSe, where the relatively shallow valence band offset gives rise to an intermediate regime. In the latter, we uncover a *step-defined pseudo-type-II* behavior for which the hole remains localized within the core despite type-II alignment which revealed by both the radial wavefunction distribution and enhanced hole transmission at thinner shells. Our results highlight the critical role of step-defined potentials in determining carrier localization and offer insight into modulating transition energies and radiative lifetimes for near-infrared optoelectronic applications.

This paper is organized as follows. The Methods section introduces the theoretical framework of the project that includes schematic energy diagrams, radial equation and transmission coefficient derivation. This is followed by the Results and Discussion section that presents numerical results for both strong and weak confinement regimes, applied to PbS/CdS and ZnTe/ZnSe heterostructures respectively, analyzing the radial probability density, transmission coefficient and the energy transition response. Finally, the last section concludes our findings and future outlooks.

## METHODS

*Theoretical Framework*

*Band Alignment and Confinement Types*

Core-shell quantum dots (CSQDs) are traditionally classified into type-I and type-II systems based on band alignment at the core-shell interface. In this study, we focus on type-II and pseudo-type-II configurations. We model carrier confinement using finite step potentials that reflect realistic band offsets. The pseudo-type-II regime arises when the valence band offset is shallow, preventing complete hole delocalization into the shell, despite a type-II band profile which is schematically described in Figure 1.

To model these behaviors, we consider two representative material systems: PbS/CdS, which exhibits strong confinement, and ZnTe/ZnSe, which demonstrates pseudo-type-II behavior due to shallower valence band offset. The material parameters used in our modeling are listed in Tables 1 and 2.

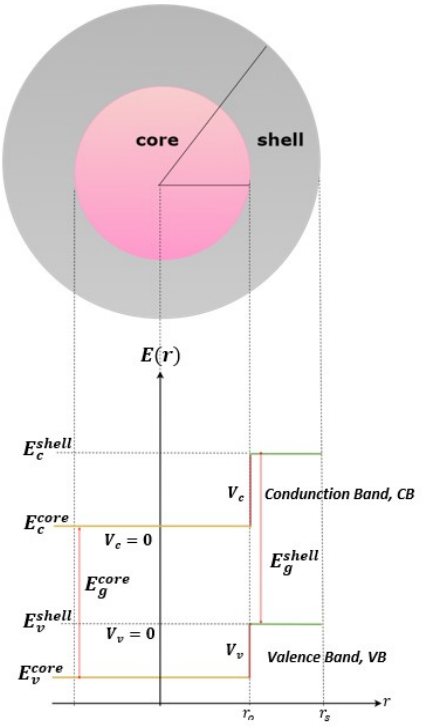


Figure 1. Schematic diagram of band line-up of Type-II CSQDs [7]

Figure 2 illustrates the band edge alignment and spatial carrier behavior for both strong and pseudo-type-II confinement regimes, supporting our classification based on step-defined potentials.

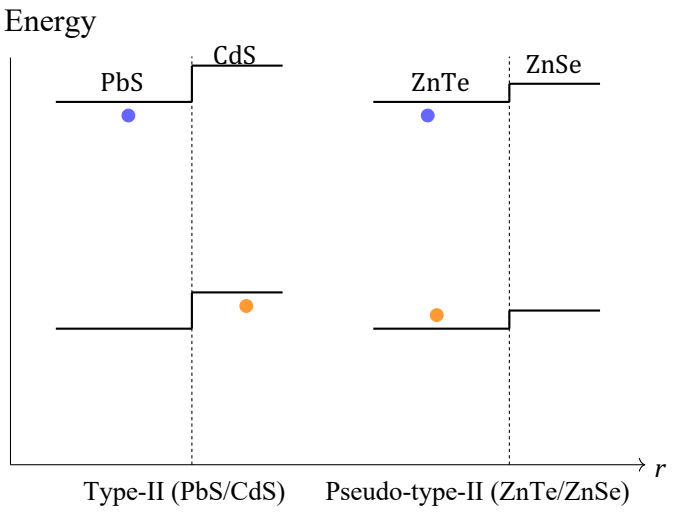


Figure 2. Band alignment comparison between type-II (PbS/CdS) and pseudo-type-II (ZnTe/ZnSe) quantum dots. Both systems exhibit upward steps in conduction and valence bands. In type-II, strong band offsets cause spatial separation of carriers, while in pseudo-type-II, shallow steps prevent full separation

Table 1. List of parameters for PbS/CdS core-shell QDs

| Materials | PbS [8] | CdS [8,9] |
|---|---|---|
| Band gap (eV) | 0.41 | 2.5 |
| $m_e/m_0$ | 0.08 | 0.2 |
| $m_h/m_0$ | 0.08 | 0.7 |
| Relative permittivity, $\varepsilon_r$ | 169 | 8.73 |
| $V_c$ (eV) | - | 2.29 |
| $V_v$ (eV) | - | 0.20 |

Table 2. List of parameters for ZnTe/ZnSe core-shell QDs

| Materials | ZnTe [8,10] | ZnSe [8,10] |
|---|---|---|
| Band gap (eV) | 2.394 | 2.8215 |
| $m_e/m_0$ | 0.11 | 0.14 |
| $m_h/m_0$ | 0.7 | 0.6 |
| Relative permittivity, $\varepsilon_r$ | 8.7 | 9.1 |
| $V_c$ (eV) | 1.6275 | - |
| $V_v$ (eV) | 1.2000 | - |

*Radial Schrodinger Equation*

In conventional type-II quantum dots, the transition energy between the lowest confined electron and hole states can be approximated using the Brus formula [11]:

$$E_{QD} = E_g + \frac{\hbar^2\pi^2}{2R^2}\left(\frac{1}{m_e} + \frac{1}{m_h}\right) - \frac{1.8e^2}{4\pi\varepsilon_0\varepsilon_r R}, \quad (1)$$

where $E_g$ is the bulk bandgap, $m_e$ and $m_h$ are the effective masses of the electron and hole, $R$ is the quantum dot radius, and $\varepsilon_r$ is the relative permittivity. This expression assumes infinite potential barriers and perfect spatial overlap of the electron and hole wavefunctions.

In core-shell quantum dots (CSQDs) with type-II alignment, however, the spatial separation between carriers and the presence of finite step-like confinement potentials require a modified approach. Here, we adopt a single-band model that incorporates [1,12]:

- Step potential barriers at the core-shell interface defined by conduction ($V_c$) and valence band offsets ($V_v$),
- Material-dependent effective masses for core and shell regions,
- Spherical symmetry and continuity of the wavefunction and its derivative at the interface.

- In this work, we solve the radial part of the single-band Schrodinger equation for spherical symmetry:

$$\left[-\frac{\hbar^2}{2m^*}\left(\frac{d^2}{dr^2}+\frac{2}{r}\frac{d}{dr}\right)+V(r)\right]R(r)=ER(r), \quad (2)$$

where $R(r)$ is the radial wavefunction, $m^*$ is the effective mass, and $V(r)$ is the step potential profile for either the electron or hole. Appropriate boundary conditions are applied at the core-shell interface and at the outer shell boundary.

*Transition Energy Model*

We define the transition energy between the lowest electron and hole states which typically approximated as

$$\Delta E_{\mathrm{QD}} = E_e + E_h, \quad (3)$$

where $E_e$ and $E_h$ are numerically obtained energy levels, relative to the conduction and valence band edges respectively. The Coulomb interaction term is neglected due to spatial separation of electron and hole wavefunctions [11]. This formulation accounts for material-dependent effective masses and finite barrier heights. The Brus equation is not applicable in this regime due to asymmetry and carrier separation. Furthermore, $\Delta E_{\mathrm{QD}}$ is the absolute transition energy with % increase calculated relative to the bulk band gap $E_g$ of the core material.

***Transmission Coefficient***

To quantify tunneling through the shell barrier, we compute the transmission coefficient $T(E)$ using the piecewise solution of the step potential model as

$$T(E)=\left[\frac{F_{transmitted}}{F_{incident}}\right]^2, \quad (4)$$

where the fluxes are computed from the radial components of the wavefunction. The transmission is energy-dependent and sensitive to shell thickness and barrier height, providing insight into carrier delocalization.

*Radial Probability Density*

The spatial confinement of carriers is further visualized using the radial probability density

$$P(r) = |R(r)|^2 r^2, \quad (5)$$

which highlights the localization region of each carrier. In pseudo-type-II systems, the hole density remains peaked in the core, in contrast to the shell-localized behavior in true type-II configurations.

## RESULTS AND DISCUSSION

Based on the theoretical framework outlined above, we now present numerical results for two representative core–shell systems: PbS/CdS and ZnTe/ZnSe. These materials were selected to exemplify distinct confinement regimes between strong type-II and step-

defined pseudo-type-II based on their step-potential profiles and band offsets. We analyze the computed radial probability densities, transmission coefficients, and resulting transition energies for both electrons and holes as functions of shell thickness. These physical quantities collectively enable us to classify the confinement behavior, assess the effectiveness of the pseudo-type-II regime, and interpret the impact on optical transition modulation. Where relevant, we refer back to Eqs. (3), (4), and (5) to highlight the physical mechanisms underlying the observed trends.

*Radial probability densities and electron–hole overlap in type-II and pseudotype-II CSQDs*

The spatial form of the electron and hole radial probability densities Eq. (5) $u(r)^2 = |R(r)|^2 r^2$ reflects the combined influence of effective masses and band offsets in core–shell quantum dots (CSQDs). Figure 3 compares PbS/CdS (type-II) and ZnTe/ZnSe (pseudo-type-II) systems, with shaded regions marking the core ($r_{core}$ = 2 nm) and shell ($r_{shell}$ = 4 nm) regions.

In PbS/CdS, the small electron effective mass and large conduction-band offset drive electron localization in the shell, while the hole having the same low effective mass, resides predominantly in the core. This strong spatial separation is characteristic of type-II alignment. In ZnTe/ZnSe, the larger hole effective mass and more moderate valence-band offset lead to a hole wavefunction that extends further into the shell, overlapping substantially with the electron. This partial carrier separation, combined with significant spatial overlap, is the hallmark of
pseudo-type-II confinement.

The degree of electron–hole coincidence was quantified using the signed radial overlap,

$$O = \int_0^\infty R_e(r) R_h(r)\, r^2\, dr, \tag{6}$$

and the normalized, dimensionless overlap,

$$S = \frac{O}{\sqrt{\int_0^\infty R_e^2(r) r^2 dr \int_0^\infty R_h^2(r) r^2 dr}}. \tag{7}$$

Here $O$ preserves the sign set by the relative phase of $R_e$ and $R_h$, whereas $|S|$ measures the magnitude of spatial coincidence. Both were evaluated from numerically computed ground-state radial wavefunctions ($l$ = 0) using a finite-difference solution of the reduced radial Schrodinger equation.

In the envelope function approximation, the radiative recombination rate scales as $\Gamma_{rad} \propto |S|$ [13,14]. ZnTe/ZnSe exhibits a ∼ 12% larger normalized overlap magnitude than PbS/CdS, implying a correspondingly higher recombination rate despite its nominal pseudo-type-II classification. This behavior shows that pseudo-type-II systems can sustain relatively high oscillator strength and emission efficiency while retaining some carrier separation. This offer a balance between lifetime extension and optical activity. Conversely, the reduced $|S|$ in PbS/CdS reflects the strong spatial separation imposed by its type-II alignment, effective mass combination, and large band offsets, which together suppress radiative recombination.

Table 3. Electron–hole overlaps for PbS/CdS (type-II) and ZnTe/ZnSe (pseudo-type-II) CSQDs from normalized radial wavefunctions. $O$ is the signed radial overlap ($nm^3$), $S$ the normalized dimensionless overlap, and the ratio is based on $|S|$

| System | $O$ ($nm^3$) | $S$ | $\|S\|$ Ratio |
|---|---|---|---|
| PbS/CdS | $-8.665 \times 10^{26}$ | −0.8665 | 1.00 |
| ZnTe/ZnSe | $9.724 \times 10^{26}$ | 0.9724 | 1.12 |

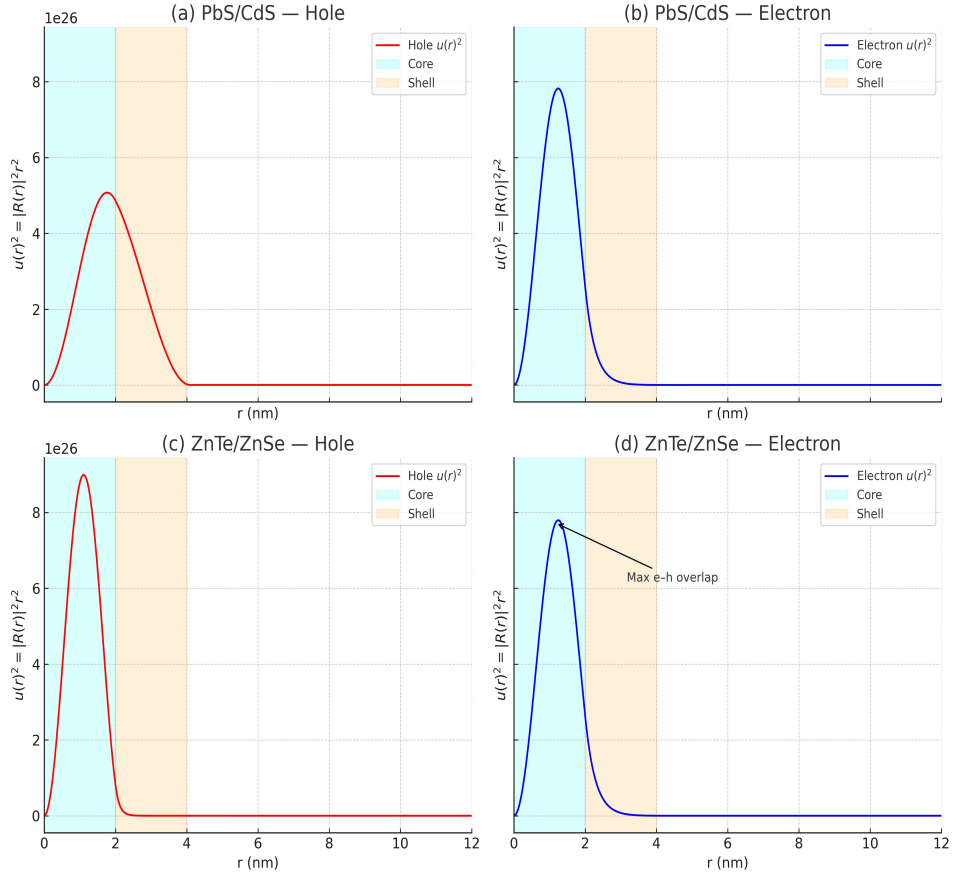


Figure 3. Radial probability density ($u(r)^2$) for both case of strong (PbS/CdS) and weak confinement (ZnTe/ZnSe) in terms of hole-electron Shaded regions indicate the core ($r_{core}$ = 2 nm, cyan) and shell ($r_{shell}$ = 4 nm, orange). The arrow in (d) marks the position of maximum electron–hole overlap in ZnTe/ZnSe. Overlap integrals are: PbS/CdS $O$ = $-8.665 \times 10^{26}$ $nm^3$, $S$ = −0.8665; ZnTe/ZnSe $O$ = $9.724 \times 10^{26}$ $nm^3$, $S$ = 0.9724. Here, $O = \int R_e(r) R_h(r) r^2 dr$ and $S = O/\sqrt{\int R_e^2(r) r^2 dr \int R_h^2(r) r^2 dr}$ (dimensionless if normalized). The sign of $O$ reflects the relative phase of $R_e$ and $R_h$, while $|S|$ quantifies the electron–hole spatial coincidence

*Transition Energy Response*

The transition energy modulation in PbS/CdS remains nearly constant across the investigated size range, reflecting strong carrier confinement and the robustness of type-II alignment following Eq. (3). In contrast, ZnTe/ZnSe exhibits a size-dependent

transition energy increase, which saturates beyond 5-7 nm (Figure 4), indicating a regime of pseudo-confinement where carriers, especially the electron, experience partial delocalization. This trend is consistent with the higher $|S|$ value reported in Table 3, which indicates stronger electron–hole spatial coincidence and thus higher recombination potential. This is consistent with our radial probability and transmission coefficient results.

The combination of radial probability profiles and transmission analysis thus allows a refined classification of confinement regimes. We propose that the term "step-defined pseudo-type-II" accurately captures the intermediate behavior in ZnTe/ZnSe systems, where carrier localization is governed not only by band offsets but also by effective mass, shell thickness, and potential step gradients.

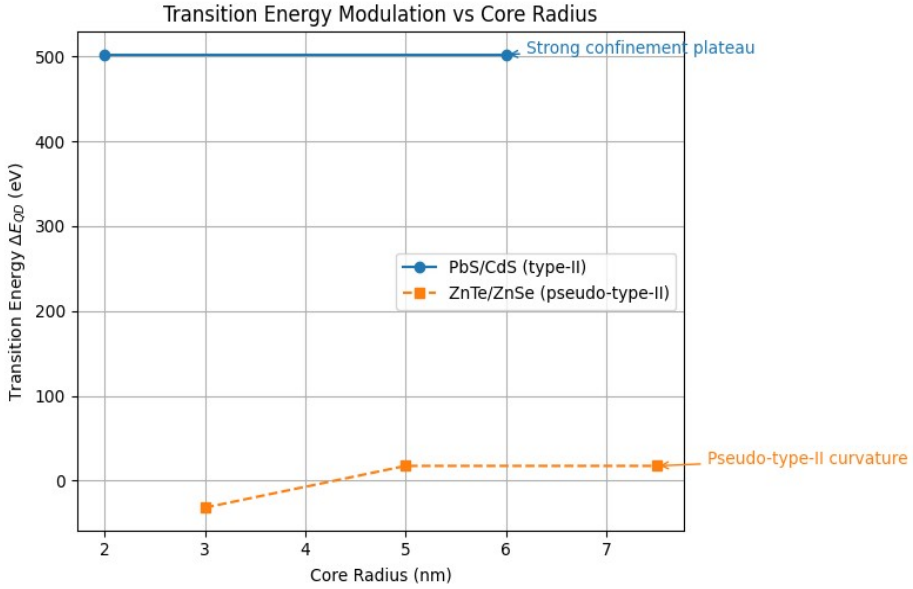


Figure 4. Comparison of transition energy modulation in PbS/CdS and ZnTe/ZnSe core-shell quantum dots. PbS/CdS exhibits strong confinement behavior with a size-independent as $\Delta E_{QD}$ increase. ZnTe/ZnSe displays pseudo-type-II characteristics with size-sensitive transition behavior that saturates at larger radii (>5 nm)

To quantify the effect of step-defined confinement on transition energy, we computed the lowest energy levels for both electrons and holes using a finite step potential model. These energy levels were summed to estimate the quantum dot transition energy $\Delta E_{qd}$, which we compared against the bulk band gap of the core material to obtain a normalized percentage increase. As shown in Table 4, for the PbS/CdS system under strong confinement, the calculated $\Delta E_{qd}$ is approximately 0.43 eV, reflecting a ~4.9% increase over the core bulk gap of 0.41 eV. This increase is attributed to the strong spatial localization of the electron within the PbS core and partial delocalization of the hole into the shell, as further confirmed by the transmission coefficient analysis and radial probability density plots.

Table 4. Summary of Confinement Behavior and Transition Energy Modulation

| System | Step Potential Depth | Carrier Behavior | $\Delta E_{qd}$ (eV) | % Increase |
|---|---|---|---|---|
| PbS/CdS | High(Strong confinement) | $e^-$ localized, $h^+$ semi-delocalized | 0.43 | 4.88% |
| ZnTe/ZnSe | Low (Pseudo-type-II) | Both $e^-$ and $h^+$ partially confined | 2.46 | 2.76% |

In contrast, the ZnTe/ZnSe heterostructure exhibits a significantly lower transition energy modulation (~2.8%), despite having a larger potential offset for the hole. This outcome reveals a pseudo-type-II regime, in which both carriers remain partially confined within the core due to the shallow step height and reduced confinement energy. Notably, the weak hole confinement leads to a transition energy only slightly above the bulk value, mimicking type-I-like overlap in a nominally type-II band-aligned system. This modulation behavior, together with spatial carrier analysis, highlights the feasibility of tuning emission energies through confinement engineering, particularly for near-infrared applications that require controlled carrier lifetimes. The shallow valence offset ($V_v$ = 1.6275 eV) and lower effective mass mismatch in ZnTe/ZnSe weaken hole confinement, resulting in near-bulk behavior. In contrast, PbS/CdS's deeper conduction offset ($V_c$ = 2.29 eV) dominates, enhancing confinement effects.

Our analysis of PbS/CdS and ZnTe/ZnSe core-shell quantum dots reveals two distinct confinement regimes driven by the depth and asymmetry of the step potential profiles. In PbS/CdS, the near-zero electron transmission coefficients ($T \approx 0$; Figure 5) reflect strong core localization due to the deep conduction barrier ($V_c$ = 2.29 eV), while elevated hole transmission ($T > 0.5$ for thin shells) confirms partial delocalization into the shell describing of type-II behavior. The low hole transmission ($T \leq 0.035$) in ZnTe/ZnSe, combined with core-localized radial densities Figure 6), arises because the shallow valence barrier ($V_v$ = 1.2 eV) lacks the energy gradient to overcome the effective mass mismatch ($0.7m_0 \rightarrow 0.6m_0$). This show pseudo-type-II characteristics that depict the radial probability density Figure 3 for a core-localized holes. This arises because the shallow valence offset ($V_v$ = 1.20 eV) and effective mass gradient ($0.7m_0 \rightarrow 0.6m_0$) kinetically trap holes despite favorable tunneling conditions. These results translated that confinement regimes cannot be classified by band alignment or transmission alone. Instead, the interplay of $T(E)$ and spatial localization defines the step-defined pseudo-type-II category.

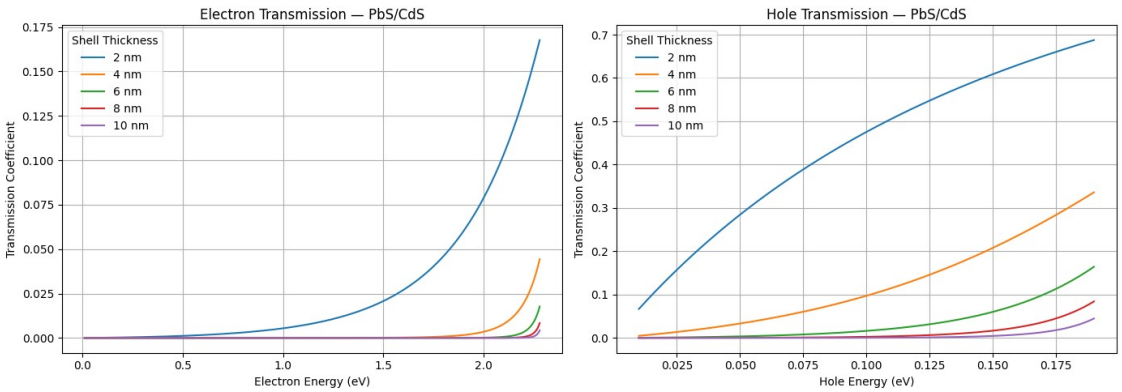


Figure 5. Combined electron and hole transmission for PbS/CdS

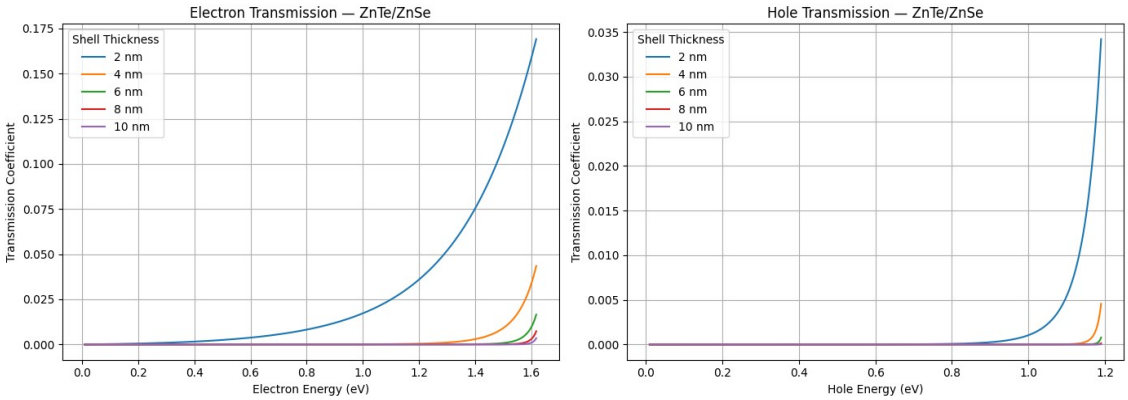


Figure 6. Combined electron and hole transmission for ZnTe/ZnSe. Maximum $T =$ 0.035 signaled a weak tunneling

The numerically computed volumetric overlaps, $S = \int |\psi_e|^2 |\psi_h|^2 dV$, are 2.008 × $10^{25}$ for PbS/CdS and 4.951 × $10^{25}$ for ZnTe/ZnSe. The significantly smaller overlap in PbS/CdS reflects strong carrier separation, consistent with a type-II regime and suppressed radiative recombination. In contrast, the ZnTe/ZnSe system exhibits more than twice the overlap, despite possessing type-II band offsets ($V_c$ = 1.6275 eV, $V_v$ = 1.2000 eV). This larger overlap arises from the combination of a shallow valence band step and moderate hole effective mass mismatch between the core and shell, which together limit hole delocalization and produce a pseudo-type-II regime with enhanced oscillator strength and reduced carrier lifetime relative to the pure type-II case.

## CONCLUSIONS

We have investigated the confinement behavior of carriers in type-II and pseudo-type-II core-shell quantum dot systems using radial probability densities and quantum transmission coefficients. For PbS/CdS, the results confirm a strong confinement regime consistent with a type-II alignment, where the electron remains localized within the core and the hole exhibits partial delocalization into the shell. The suppressed electron-hole overlap and energy-dependent tunneling behavior support this classification.

In contrast, the ZnTe/ZnSe system exhibits characteristics of a pseudo-type-II configuration. Despite possessing staggered band offsets suggestive of type-II alignment, the hole remains localized in the core due to the shallowness of the valence band offset and the step-defined potential. This behavior is evident from both the high radial probability density in the core and the elevated transmission coefficient for holes, particularly at thinner shell widths.

These results highlight the importance of combining radial and transport analyses to go beyond simple band alignment classifications. We introduce the term *step-defined pseudo-type-II* to describe systems where the apparent type-II offset is insufficient to enforce spatial separation of carriers. This classification is especially relevant for ZnTe/ZnSe and other systems with asymmetric confinement behavior. Our framework provides a useful basis for interpreting experimental photoluminescence shifts and designing tailored QD systems for optoelectronic applications [15].

## ACKNOWLEDGMENTS

This work is partly funded by UPM/GP grant 9752900.

## AUTHORS' CONTRIBUTIONS STATEMENT

The manuscript was written through the contributions of all authors. N.A.A.A.H. and N.M.S designed and organized this work. N.M.S. drafts the main ideas of the work. C.K.T. and A.R. review and editing of the manuscript. All authors have approved the final version of the manuscript.

## CONFLICT OF INTEREST

All authors declare no competing interests that could have influenced the work reported in this paper.

## REFERENCES

1. Du N, Chen H. First principles study of quantum dots-sensitized solar cells using type-II core/shell quantum dots as efficient sensitizers. *Computational Materials Science.* 2024;232:112654.
2. Khan W, Watts A, Green M. Simple all-inorganic electroluminescent devices based on type-II CdTe/CdS/ZnS core/shell/shell quantum dots. *Asian Journal of Applied Sciences.* 2014;2(3).
3. Aghoutane N, Pérez LM, Laroze D, El-Yadri M, Feddi EM. Importance of core and shell sizes in the localization of the electron and hole in the formation of type-I or type-II excitons in spherical CdSe/ZnTe and CdSe/CdTe quantum dots. *Results in Physics.* 2022;44:106158.
4. Tiansin S, Nurisya MS, Tim CK, Mazliana AK. Effects of step-potential on confinement strength of strain-induced type-I core-shell quantum dots. *Superlattices Microstructure*. 2019;131:95–103.
5. Kim S, Fisher B, Eisler H, Bawendi M. Type-II quantum dots: CdTe/CdSe (core/shell) and CdSe/ZnTe (core/shell) heterostructures. *Journal of the American Chemical Society*. 2003;125(38):11466–11467.
6. Simi NJ, Tom AE, Vinayakan R, Ison VV. Photoinduced charge transfer studies of type-II core-shell ZnTe–ZnSe quantum dots. *Journal of Nanoparticle Research*. 2020;22:135. doi:10.1007/s11051-020-04851-5.
7. Tiansin S, Nurisya MS, Jellal A. Confining type-II spherical core-shell quantum dot heterostructures with narrow and wide band gaps. *arXiv*. 2021;2111.14378v1.
8. Mishra UK, Singh J. *Semiconductor Device Physics and Design*. Dordrecht: Springer Netherlands; 2008.
9. Madelung O, Rössler U, Schulz M. *Semiconductors II-VI and I-VII Compounds; Semimagnetic Compounds: Cadmium Sulfide (CdS) Dielectric Constants*. Berlin: Springer; 1999.

10. Jia G, Hao B, Lu X, Yao J. Size effect of heterostructure type in core/shell quantum dots. *International Journal of Electrochemical Sciences*. 2013;8:8167.
11. Brus LE. Electron-electron and electron-hole interactions in small semiconductor crystallites: the size dependence of the lowest excited electronic state. *Journal of Chemical Physics*. 1984;80(9):4404.
12. Pistol ME, Pryor C. Band-edge diagrams of core-shell semiconductor dots. *Journal of Physical Chemistry C*. 2011;115(22):10931–10939.
13. Efros AL, Efros AL. Interband absorption of light in a semiconductor sphere. *SPIE Milestone Ser*. 2005;180:71–74.
14. Zanolli Z, Pistol ME, Fröberg LE, Samuelson L. Quantum-confinement effects in InAs–InP core–shell nanowires. *Journal of Physics:Condensed Matter*. 2007;19:295219.
15. Li D, Huang K, Zhang F, Li J, Liu Y, Cheng T. ZnTe/ZnSe core-shell type quantum dot and preparation method thereof. Patent, 2016.